The Journal of Supercritical Fluids 234 (2026) 106970

Contents lists available at ScienceDirect

The Journal of Supercritical Fluids

journal homepage: www.elsevier.com/locate/supflu

A two-step regeneration method for carbon-supported Ru catalysts deactivated by coke and sulfur during hydrothermal gasification

Songlan Sun [a], Saša Bjelić [b], Weicheng Hua [b], Frédéric Vogel [a,b,*], David Baudouin [b]

[a] University of Applied Sciences Northwestern Switzerland (FHNW), School of Engineering and Environment, 5210 Windisch, Switzerland
[b] Paul Scherrer Institute (PSI), Center for Energy and Environmental Sciences, PSI, CH-5232 Villigen, Switzerland

HIGHLIGHTS

- Two-step aqueous regeneration restores Ruthenium catalyst activity.
- Low-temperature H_2O_2 oxidation removes coke and converts sulfur to oxidized forms.
- Subcritical water flushing desorbs strongly bound sulfur species.
- 97 ± 2% sulfur removal achieved without damaging carbon support.
- Enables catalyst regeneration and lifetime extension without reactor disassembly.

GRAPHICAL ABSTRACT

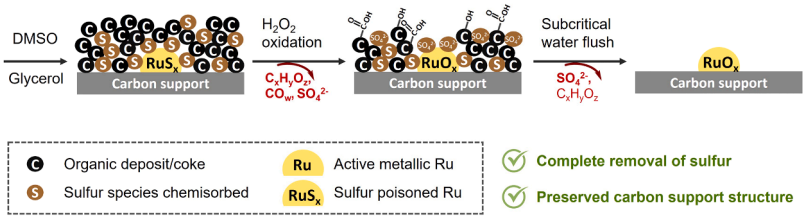

ARTICLE INFO

Keywords:
Catalytic hydrothermal gasification
Catalyst regeneration
Coke deposition
Sulfur poisoning
Catalyst deactivation

ABSTRACT

Catalytic hydrothermal gasification (cHTG) offers a sustainable pathway for converting wet biomass into methane, but long-term operation is hindered by catalyst deactivation, particularly due to coke deposition and sulfur poisoning. Ruthenium on activated carbon (Ru/AC) is highly active for methane production but gradually loses performance during continuous gasification of biomass or wastes. Conventional high-temperature oxidative regeneration methods, which rely on combustion to remove coke, are unsuitable for carbon supports due to their poor stability in the presence of oxidizing agents at high temperatures. Here, a low-temperature aqueous regeneration strategy was explored using hydrogen peroxide (H_2O_2) oxidation followed by subcritical water flushing. Effluent analysis and catalyst characterization reveal that coke is primarily oxidized and removed during H_2O_2 oxidation (<120 °C), while sulfur species are oxidized to strongly adsorbed forms (sulfate) that require subsequent desorption via subcritical water flushing. Based on these insights, a two-step regeneration protocol was developed, consisting of two H_2O_2 oxidation treatments (85–120 °C), each followed by subcritical water flushing (up to 320 °C). This approach achieves (97 ± 2) % sulfur removal while preserving carbon support integrity. The method enables efficient catalyst regeneration targeting both coking and sulfur fouling, offering a practical aqueous strategy to extend the operational lifetime of Ru/AC catalysts in cHTG and related catalytic systems without the need to remove the material from the catalytic reactor for regeneration.

* Corresponding author at: University of Applied Sciences Northwestern Switzerland (FHNW), School of Engineering and Environment, 5210 Windisch, Switzerland.
E-mail address: frederic.vogel@psi.ch (F. Vogel).

https://doi.org/10.1016/j.supflu.2026.106970
Received 7 November 2025; Received in revised form 13 March 2026; Accepted 16 March 2026
Available online 18 March 2026

1. Introduction

Catalytic hydrothermal gasification (cHTG) is a promising technology for converting wet organic waste into clean energy carriers such as methane or hydrogen under supercritical water conditions. A key challenge is catalyst deactivation caused by specific components in biomass feedstock [1,2], which can only be partially mitigated through the use of a sulfur scavenger. This deactivation, closely tied to the catalyst cost, significantly impacts the CAPEX of a cHTG plant.

Ruthenium supported on high-surface-area activated carbon (Ru/AC) has shown the highest activity and stability for selective methane production in cHTG [3]. Nevertheless, this catalyst may gradually deactivate during long-term continuous operation [4]. Deactivation can occur via several mechanisms [1,3], including poisoning by impurities such as sulfur or transition metals [5], fouling due to coke or salt deposition [6,7], sintering of the active phase [8,9], structural changes in the catalytic material [10], or mechanical and chemical loss of the active component [4]. Ruthenium sintering is minimal under typical cHTG conditions [5,11], and leaching is also negligible due to the extremely low solubility of both metallic Ru and Ru oxides in supercritical water (SCW) [4,12]. However, mechanical loss of the catalyst can occur during abrupt fluctuations in feed rate or pressure, leading to the release of catalyst fragments [4]. While this mode of Ru loss can be critical under unstable conditions or during harsh oxidative treatments [13], it is usually not observed during steady-state operation.

Among the various causes of catalyst deactivation under cHTG conditions, coking and poisoning are the most prevalent and persistent during biomass conversion. These forms of deactivation are typically caused by the presence or by the favored formation of recalcitrant aromatic and organosulfur compounds, respectively [14–16]. Catalyst deactivation by coke occurs through coverage of active sites and blockage of pores, which restricts mass transport and adsorption. Recent mechanistic insights using glycerol as a model compound reveal that coke originates from unsaturated aliphatic and aromatic intermediates formed via aldol condensation, cyclization, and dehydrogenation [15]. These species condense into nanometric carbon layers [17], up to 10 nm thick [15], on catalyst surfaces, significantly reducing metal accessibility and activity. While glycerol is a clean model, real biomass contains more diverse and variable constituents, such as lignin-derived aromatics, lipids, and proteins, which can exacerbate coke formation and make deactivation more severe in practice.

Sulfur-containing contaminants, originating for instance from sulfur-containing amino acids, lipids or co-enzymes, are inherently present in most biomass sources. Under cHTG conditions, sulfur in various forms readily deactivates Ru-based catalysts [5,11]. For example, the formation of ruthenium sulfide (S(-II)) was evidenced by *ex situ* sulfur K-edge XANES [5], resulting from the reduction of dimethyl sulfoxide (S(+II)) under cHTG conditions. Sulfur species with oxidation states from -II to 0 readily adsorb on the Ru surface via chemisorption or form Ru sulfides after C-S bond cleavage, strongly affecting the catalytic activity of the metal surface [5]. Although sulfate is typically considered a stable species, under cHTG conditions it becomes thermodynamically prone to reduction into sulfide via thermochemical sulfate reduction (TSR) [18]. The kinetics of this transformation are notably slow compared to typical process timescales [19] and the solubility of sulfate under cHTG conditions is low [20]. However, TSR remains a problem because catalyst deactivation can still occur at a sulfate concentration as low as 16 ppm [11], possibly by a Ru-catalyzed reaction [18,21]. To protect the catalyst from sulfur poisoning, various affordable sulfur scrubbing materials can be installed upstream of the catalyst bed, active absorbing materials including nickel metal [22], ZnO [23,24], CuO [16,25], or CeO_x[25] (x indicating variable oxidation states). However, despite the very low solubility of sulfur salts in SCW [20] and the high sulfur absorption equilibrium constant achievable with some sulfur-absorbing materials, small concentrations of sulfate [20] and organosulfur compounds [16] can still reach the catalyst bed. With time, sulfur will therefore accumulate in the catalyst bed, a process that can be accelerated by flow anomalies such as channeling or bypassing in the sulfur scrubber, or by high concentrations of recalcitrant organosulfur compounds, such as thiophenes [16], methylthiol, and dimethyldisulfide [16].

Ruthenium is a costly metal, and for that reason regenerating the deactivated catalyst is essential for the economic viability of cHTG. Coke-induced deactivation is generally reversible, and in most industrial processes, it is addressed by oxidizing the deposits with air at temperatures above 400 °C [26]. Alternative strategies have been developed specifically for carbon-based systems. These include low-temperature oxidation using ozone [27] or hydrogen peroxide [13], steam or CO_2 gasification [26], non-oxidative treatments such as pyrolysis or hydrogenation [28,29], and solvent-based [30–32] or supercritical fluid extraction [33].

A regeneration strategy that can effectively address both coke and sulfur deactivation in carbon-supported catalysts is highly desirable. Some of the approaches developed for coke removal can also be applied to sulfur poisoning. Gaseous oxidative treatments aim to convert sulfur into volatile SO_x gases or sulfates [34], while reductive treatments with hydrogen [35] or ammonia target conversion to H_2S or decomposable ammonium salts (e.g., $(NH_4)_2SO_4$) [36]. Yet, these gaseous treatments often fail to fully remove sulfur contaminants, especially when they are strongly chemisorbed or converted into non-volatile sulfates [34,35]. An alternative strategy targets sulfur removal through water-based treatments, specifically subcritical water. Subcritical water is hot and pressurized liquid water below the critical point of water (374 °C, 22.1 MPa). In this regime, the ionic product of water (Kw) increases markedly, influencing solvation behavior and interfacial chemistry [37]. In addition, elevated temperature enhances mass transfer and diffusivity [38], while the dielectric constant of water decreases relative to ambient conditions. Although the reduced dielectric constant under subcritical conditions lowers the solubility of many inorganic salts, sulfate species remain sufficiently soluble to be removed once desorbed from the catalyst surface [39]. Importantly, sulfur removal is not limited by solubility, but is primarily governed by thermally activated desorption of strongly adsorbed sulfur species. Elevated temperature provides the driving force for desorption, while sufficient solvation capacity enables subsequent removal by aqueous flushing. For example, subcritical water treatment at 300 °C and 25 MPa removed approximately 70% of the sulfur from a poisoned Ru catalyst and restored around 50% of its original activity [40], probably as a result from Ru sulfide oxidation and subsequent flushing of the sulfate. Other studies have reported that hot water washing [41–44] can outperform conventional thermal regeneration methods in restoring different catalytic systems poisoned by various forms of sulfur (e.g., H_2SO_4, SO_2).

As an aqueous oxidant, hydrogen peroxide (H_2O_2) not only oxidizes carbonaceous deposits (coke) and transforms various sulfur species into soluble or releasable forms such as sulfates and bisulfate [45], but also enables straightforward integration with subcritical water flushing, facilitating the direct removal of water-soluble sulfates. Moreover, H_2O_2 has been shown to cleave Ru–S bonds and oxidize Ru to RuO_2 under mild conditions (RuO_2 predominates above 50 °C and fully forms above 110 °C), as observed via EXAFS [13]. Nevertheless, its application to Ru/AC regeneration has revealed trade-offs: treatments below 125 °C are less effective against sulfur poisoning, while higher temperatures ($\geq$ 125 °C) cause structural damage to the carbon support [13]. Two-step sequences under milder conditions ($<$ 120 °C) with intermediate water rinsing can restore about 85% of the catalytic activity, yet the role of the water rinse, the fate of sulfur species, and the persistence of incomplete recovery and rapid re-deactivation upon reuse remain unresolved.

In this work, we advance beyond earlier demonstrations of two-step H_2O_2 regeneration by elucidating how oxidation and the desorption of carbon- and sulfur-containing species jointly contribute to restoring the activity of Ru/AC catalysts deactivated by coke and sulfur under cHTG conditions. Effluent analysis enables direct tracking of sulfur and coke

release, providing insights into how the two steps act in tandem. This work identifies subcritical-water flushing as the previously unrecognized step that enables near-complete sulfur removal following H_2O_2 oxidation, by desorbing oxidized sulfur species strongly bound to the Ru/AC surface. This understanding clarifies why previous H_2O_2 treatments were suboptimal and establishes a practical route to extend catalyst lifetime in biomass cHTG, with broader potential for regenerating metal-on-carbon catalysts in other reaction systems.

2. Experimental methods

2.1. Chemicals and materials

5 wt% Ru supported on activated carbon (Ru/AC), RCAT®-8830 RW from Ranido (Lot No. D210226); Glycerol, ≥ 99%, anhydrous, Carl Roth; 2-propanol, ≥ 99.5%, Carl Roth; H_2O_2, 30%, stabilized, Carl Roth; dimethyl sulfoxide (DMSO), ≥ 99.9%, Sigma Aldrich; Acrylic acid coked Ru/AC is provided by TreaTech.

2.2. Analytical methods

All gas compositions were analyzed using an INFICON EZ IQ 3000 Micro-GC equipped with a thermal conductivity detector (TCD).

The carbon content of aqueous samples was analyzed using a DIMATOC® 2000 analyzer, which enables the quantification of total inorganic carbon (TIC), total carbon (TC), and total organic carbon (TOC).

Total sulfur leached into the effluent was determined by inductively coupled plasma optical emission spectrometry (ICP-OES), while sulfate was quantified spectrophotometrically using commercial test kits (Macherey-Nagel NANOCOLOR Sulfat LR 200).

The coke and sulfur-containing deposits on the deactivated catalyst were extracted and analyzed by ultra-high-performance liquid chromatography coupled with high-resolution mass spectrometry (UHPLC–HRMS).

Further details on all analytical methods are provided in SI Sections 2 and 3.

2.3. Catalyst characterizations

Nitrogen physisorption measurements were carried out using an *Autosorb iQ* surface characterization analyzer (Quantachrome Instruments). All samples were degassed at 120 °C under vacuum ($<10^{-3}$ mbar) for 10 h prior to analysis. Adsorption isotherms were collected at 77 K using liquid nitrogen.

The sulfur residue on the catalyst was determined by ICP-OES.

The surface chemical states of sulfur, oxygen, and ruthenium on the catalyst during sulfur poisoning and regeneration were investigated by X-ray photoelectron spectroscopy (XPS), with experimental and fitting details provided in SI Section 4.3.

Further details on all catalyst characterizations are provided in SI Section 4.

2.4. Experimental setup

The gasification experiments were conducted in a continuous cHTG setup named KONTI-1. Liquid feedstocks were pressurized to approximately 25 MPa and preheated before entering a fixed-bed tubular reactor containing the Ru/AC catalyst. During gasification experiments, the reactor temperature was typically maintained at around 400 °C, while lower temperatures (80–120 °C) were applied during oxidative regeneration studies.

Downstream of the reactor, the effluent was rapidly cooled, depressurized, and separated into gas and liquid phases. Gaseous products were continuously analyzed using a micro gas chromatograph, while liquid effluents were collected for off-line carbon and sulfur analyses.

To enable time-efficient regeneration studies, a second, smaller continuous setup was constructed. This setup allowed heating and pressurization under conditions comparable to KONTI-1 but without in situ gas analysis. Electrical conductivity at the reactor outlet was monitored online as an indicator of ionic species removal during regeneration.

Simplified flow diagrams of both experimental setups are provided in Figures S3 and S4, and detailed descriptions are available in Supporting Information Section 5.

3. Results and discussion

3.1. Qualification of coke and sulfur deposits

To understand the cause of Ru/AC catalyst deactivation, identifying and characterizing the nature of coke and sulfur-containing deposits is essential. The deactivation of Ru/C catalysts by model compounds has been extensively investigated [15,17,46]. Here, a commercial 5 wt% Ru/AC catalyst (RCAT®-8830 RW, Ranido), deactivated during continuous operation using an industrial monomer-containing waste stream originating from butyl acrylate production, was analyzed.

The industrial feed was fully converted during the first 16 h, mostly into CH_4, H_2, CO_2, and CO with a composition ruled by thermodynamics [47]. The gas production during these 16 h on stream was stable. However, a sharp decline in gas flow thereafter indicated catalyst deactivation. The deposits on the deactivated catalysts from the upstream, midstream, and downstream parts of the reactor were extracted with a mixture of four organic solvents, and further analyzed by UHPLC-HRMS. Experimental details can be found in the SI section 3.

Fig. 1 presents kernel density plots of double bond equivalents (DBE) versus molecular weight (MW) for all detected compounds, along with Van Krevelen diagrams (molar ratios of H/C vs. S/C) for sulfur-containing species. The data clearly show that the midstream and downstream sections of the reactor bed exhibit similar chemical compositions. The DBE maxima are around 2. Notably, DBE values increase with molecular weight. This trend indicates a consistent molecular distribution, suggesting a shared origin and/or molecular transformation pathway within the midstream and downstream sections of the reactor. The same observation holds for van Krevelen plots of the sulfur-containing species. The distribution is broad in both H/C and S/C directions, indicating that sulfur is present in a variety of molecules, including aliphatic and aromatic species.

In contrast to the midstream and downstream sections of the reactor, the upstream section exhibits distinct features in terms of the molecular weight distribution and DBE values: molecular weight reaches up to 600 g mol^{-1}; a pronounced maximum is observed at 180 g mol^{-1} with a DBE value of 4. This maximum is accompanied by two local maxima. The first is around 360 g mol^{-1} and DBE of 4, indicating large saturated species. The second one is at 220 g mol^{-1} and DBE of 10, indicating the presence of a substantial fraction of unsaturated molecular species. The Van Krevelen plot sheds deeper light on the chemical nature of the maxima, indicating a large portion of sulfur-containing aromatic species around S/C = 0.1 and H/C = 0.7, and aliphatic species at S/C = 0.1 and H/C = 1.5.

These plots reveal that during the supercritical water gasification, sulfur-containing aromatic compounds are deposited on the surface of the Ru catalyst, which could have formed through a series of aldol condensation, cyclization, and dehydrogenation reactions [15], forming a broad spectrum of S-containing aromatic compounds (“coke”).

3.2. Screening regeneration method

To ensure standardized and controlled catalyst deactivation, all subsequent experiments were conducted using the same commercial catalyst: 5 wt% Ru supported on activated carbon (Ru/AC), RCAT®-8830 RW from Ranido, and the same deactivation protocol. The

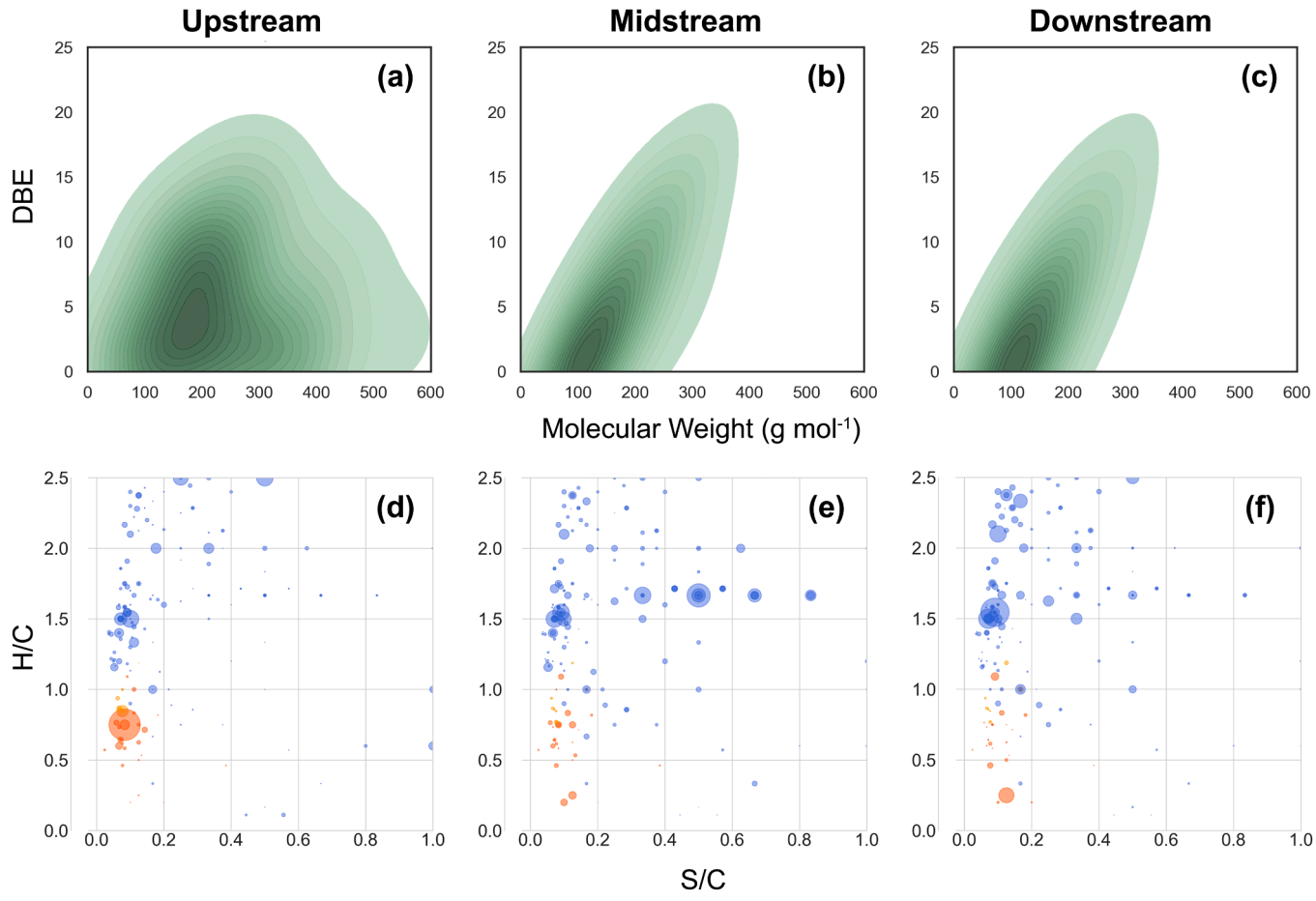

Fig. 1. (a-c) Kernel density plots of the double bond equivalent (DBE) vs. molecular weight (MW), and (d-f) Van Krevelen plots of sulfur-containing species for the Ru/AC catalyst deactivated by an industrial feedstock. (a) and (d) correspond to the upstream section of the catalytic reactor bed, (b) and (e) to the midstream, and (c) and (f) to the downstream. The dots are colored according to the aromaticity index: blue, aliphatic; orange, aromatic.

catalytic performance was evaluated based on the carbon-based gasification efficiency (Equation S1).

Deliberate deactivation by sulfur poisoning and coking was achieved by feeding a solution of 20 wt% glycerol with 500 ppm dimethyl sulfoxide (DMSO) for 1 h, followed by an additional 1 h of 20 wt% glycerol to promote further coking and to purge weakly adsorbed sulfur species. This procedure was used in each deactivation cycle unless otherwise specified (some experiments used 10 wt% isopropanol). After poisoning, carbon gasification efficiency (GEc) dropped from 80% to 99% (depending on the weight hourly space velocity) to below 10% when tested with sulfur-free 20 wt% glycerol as feed. Initially, the gas composition was CH_4: 44–56%, H_2: 4–13%, CO_2: 33–40%, and CO: 0.4–8%. After poisoning, it shifted to CH_4: 4%, H_2: 29–33%, CO_2: 9%, CO: 45–46%, and C_2H_6: 2–6%). Surface characterization of the spent catalyst after a single deactivation cycle showed a decrease in specific surface area (SSA) from 1021 $m^2\ g^{-1}$ to 758 $m^2\ g^{-1}$ and in pore volume from 0.437 $cm^3\ g^{-1}$ to 0.344 $cm^3\ g^{-1}$. A severely coked catalyst, unaffected by sulfur poisoning, was prepared by feeding acrylic acid, which is prone to polymerization or crosslinking due to its double bond and carboxyl group. The resulting GEc obtained with this coked catalyst was approximately 40% with 20 wt% glycerol (CH_4: 33%; H_2: 20%; CO_2: 26%; CO: 18%). In this case, the SSA decreased drastically from 1021 $m^2\ g^{-1}$ to 6 $m^2\ g^{-1}$, and the pore volume was nearly zero, indicating complete pore blockage by coke.

First, various regeneration approaches, including H_2 reduction, solvent extraction, and H_2O_2 oxidation, were tested on Ru/AC catalysts deactivated by a combination of coke and sulfur, or coke alone, as described above. The experiment codes, corresponding regeneration methods, operating conditions, and deactivation causes are summarized in Fig. 2. The regeneration efficiency was evaluated based on the recovery of GEc, defined as the GEc of the regenerated catalyst relative to that of the fresh catalyst (Equation S2).

H_2 reduction is effective in removing so-called "soft coke" (H/C ratio $>$ 1, mainly aliphatic and single-ring aromatics) [26,48,49] through hydrogenation [26,28]. Operation temperatures of 400 °C to 450 °C are typically applied for this purpose [28,50]. However, "hard coke" (H/C ratio $<$ 1, consisting of polycyclic aromatic hydrocarbons) requires higher temperature ($>$ 500 °C) and pressure ($>$ 15 MPa) for effective removal [50–52], which can initiate gasification of carbon support, especially in the presence of supported noble metals [53,54].

In this study, H_2 treatment at 450 °C (5 vol% H_2 in N_2, 1 atm) of a sulfur- and coke-deactivated catalyst achieved only 62% GEc recovery. This limited recovery suggests that not all deactivating species were removed under the applied conditions. As further increases in temperature could damage the carbon support, and given that oxidative treatments have been reported to be more effective for coked catalysts [52,55], an oxidative regeneration approach was explored [50,53] using an aqueous oxidant (3 wt% H_2O_2) at 25 MPa (the same pressure as used in the hydrothermal gasification tests) and 80 °C for 1 h. This treatment notably improved the GEc recovery, reaching 86% (Figure S5).

Solvent extraction, applied to a coked catalyst (coked by acrylic acid-containing industrial wastewater; see Figure S6) proved ineffective, as no improvement in GEc was observed. In fact, the GEc declined to 52% with 10 wt% 2-propanol (IPA), compared to 66% for the non-extracted coked catalyst. This decline may be attributed to partial dissolution and redistribution of organic deposits, which exacerbated active site

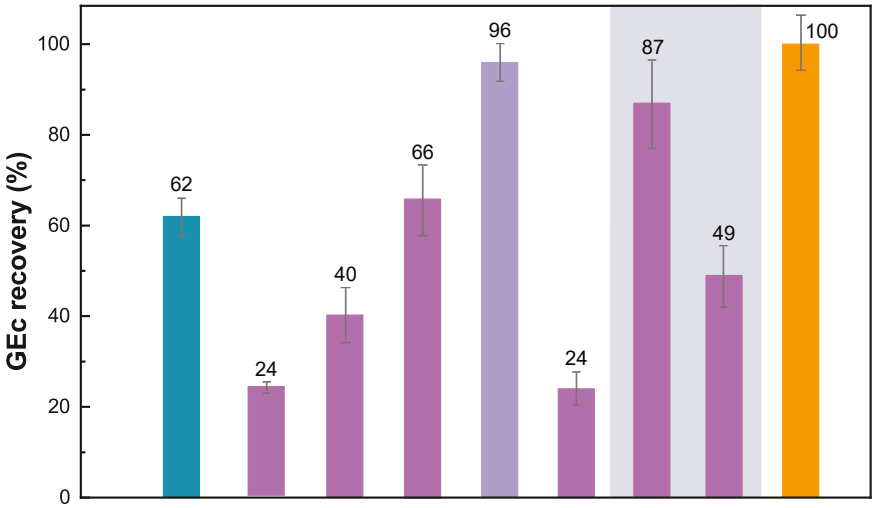

Exp. code	1-H_2	2-H_2O_2	3-H_2O_2	4-H_2O_2	5-H_2O_2*	6-H_2O_2	7-H_2O_2-cycle 3	7-H_2O_2-cycle 7	8-H_2O_2
Methods	H_2 reduction	1-step H_2O_2 oxidation							2-step H_2O_2
Conditions	450 °C, 2 h	25 °C, 60 min	72 °C, 45 min	82 °C, 50 min	80 °C, 50 min	82 °C, 60 min, 10 bar	100 °C, 60 min	100 °C, 60 min	85 °C, (35+25) min
Deactivation modes	Coke + Sulfur				Coke	Coke + Sulfur			
Deactivation causes	Via glycerol + DMSO				Via acrylic acid	Via glycerol + DMSO			

Fig. 2. Various regeneration conditions applied to deactivated Ru/AC. Performance tests were conducted by continuous hydrothermal gasification of 20 wt% glycerol in water. Sulfur poisoning was induced by adding 500 ppm of DMSO to the 20 wt% glycerol solution, while coking alone was induced by feeding acrylic acid. Exp. code refers to the experiment code. *5-H_2O_2: The H_2O_2 treatment was conducted following the activity test after solvent extraction. Further details are provided in Fig. S6. 7-H_2O_2: The first two cycles were performed at full conversion, so GEc recovery calculation could not be applied. For the other tests listed in Fig. 2, GEc before and after regeneration was measured away from thermodynamic equilibrium. Error bars represent the standard deviation of GEc within the 2-hour averaging window of a single run, not replicate uncertainty.

blockage (see SI S6.2.2 for further discussion). When a one-step H_2O_2 oxidation (25 MPa, 80 °C, 1 h) was subsequently applied to the same coked catalyst, GEc recovered to 96% (Exp. 5-H_2O_2). BET analysis further confirmed the restoration of specific surface area (from 6 $m^2\ g^{-1}$ to 751 $m^2\ g^{-1}$) and pore volume (from 0.010 $cm^3\ g^{-1}$ to 0.326 $cm^3\ g^{-1}$), indicating that H_2O_2 effectively removes coke (Table S3).

Given the effectiveness of H_2O_2 oxidation in addressing both coke deposition and sulfur poisoning, the effects of regeneration conditions, including temperature, duration, and pressure were systematically investigated (Fig. 2). During these experiments, the H_2O_2 concentration was kept at 3 wt% based on prior literature [13] and selected as a representative moderate oxidative condition. This choice is also supported by safety considerations, as higher concentrations increase the risk of uncontrolled exothermic catalyst oxidation, particularly at large scale.

GEc recovery increased progressively with temperature: at 25 °C, recovery reached approximately 24% (exp. 2-H_2O_2); at 70 °C, 40% (exp. 3-H_2O_2); and at 80 °C, it increased to 66% (exp. 4-H_2O_2). Regeneration was also strongly affected by the severity of deactivation. For a heavily poisoned catalyst that had experienced multiple incomplete low-temperature regenerations and repeated sulfur exposure (Figure S8), residual sulfur and coke likely accumulated, so even treatment at 100 °C and 25 MPa in the final regeneration cycle was ineffective.

All treatments up to this point were performed at 25 MPa, the same pressure as the hydrothermal gasification tests for ease of operation. Lowering the pressure to 1 MPa at 80 °C (exp. 6-H_2O_2) led to a much lower GEc recovery of 24%. These results suggest that oxidation efficiency may be closely linked to the dissolved oxygen concentration, known from wet oxidation to have a direct impact on reaction rates [56, 57]. The generated oxygen partitions between the gas and aqueous phases according to the gas-liquid equilibrium ($O_2(g) \rightleftharpoons O_2(aq)$), with the O_2(aq) concentration proportional to its partial pressure in the gas phase (Henry's law). Elevated pressure thus increases O_2(aq), sustaining a more effective oxidative environment. During regeneration, H_2O_2 decomposes into water and oxygen, both thermally and catalytically, likely with Ru acting as catalysts [58,59], since purely thermal decomposition is kinetically slow [60]. When Ru sites are fully covered (severely deactivated) as shown in Figure S8, decomposition slows down, limiting oxygen generation and thereby reducing the oxidation of coke and sulfur.

Additionally, when catalyst deactivation was caused solely by coking, treatment at 80 °C with H_2O_2 recovered up to 96% of the initial GEc (Exp. 5-H_2O_2), compared to 66% when both sulfur and coke were present, suggesting that addressing both types of deactivation requires higher treatment temperatures. Increasing the temperature to 100 °C (Exp. 7-H_2O_2, Fig. 3) improved regeneration, yielding 87% GEc recovery in cycle 3. The first two cycles were operated at full conversion with 10 wt% IPA (Figure S7). Since full conversion prevents quantification of GEc recovery, we replaced the feedstock with 20 wt% glycerol (instead of 10 wt% IPA) in subsequent experiments to operate in the kinetic regime.

Given the effective regeneration observed, multiple deactivation–regeneration cycles using H_2O_2 treatment at 100 °C were conducted (Fig. 3). As mentioned above, in the first cycle, the coked catalyst was regenerated and achieved nearly complete conversion. In the second cycle, a coked and sulfur-poisoned catalyst also reached full conversion (Figure S7). In the third cycle, the GEc recovery was 87%. The GEc recovery remained above 80% for the first five cycles but declined to 50% by cycle seven.

The gas production rate during each sulfur-free glycerol gasification test gradually decreased, accompanied by a slight shift in gas composition, with less CH_4 while H_2 increased (gas composition is conversion-

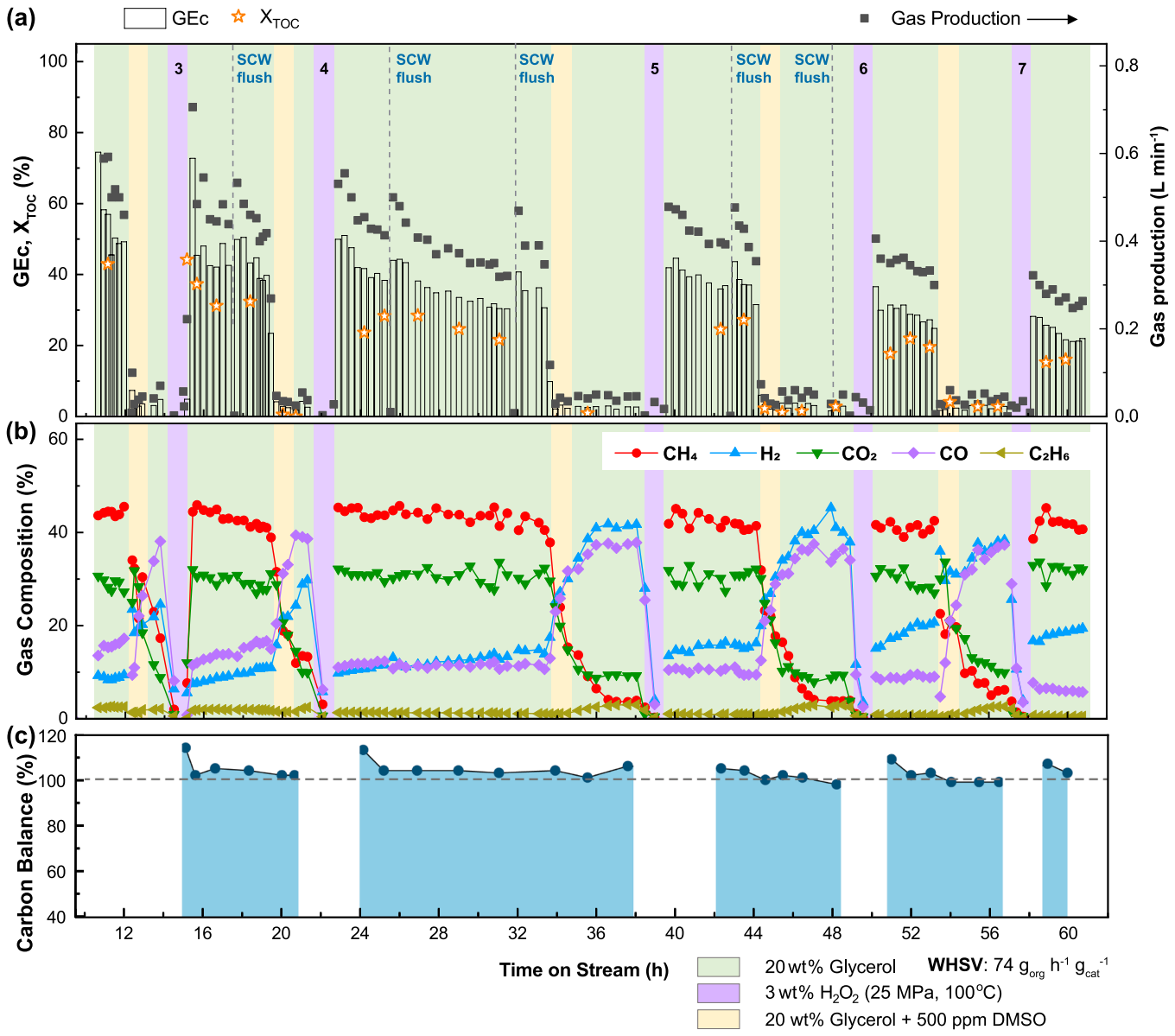

Fig. 3. 7-H_2O_2: Seven cycles of deactivation-H_2O_2 regeneration-activity testing. The first two cycles were performed under full conversion with 10 wt% IPA as the feed (data not shown here, but available in SI Fig. S7). (a) Gasification efficiency (GEc), organic carbon conversion (X_{TOC}), and gas production; (b) gas compositions obtained during the deactivation-regeneration-activity cycles; (c) the corresponding carbon balance. All hydrothermal gasification tests and poisoning were conducted under 400 °C and 25 MPa. Water flushing steps after H_2O_2 treatment are not considered as time on stream. X_{TOC} is organic carbon conversion based on total organic carbon (TOC) measured in the feed and effluent (Equation S3). Carbon balance (%) is calculated as the total carbon found in the gas and liquid phases divided by the carbon content of the feed (Equation S4). The dashed line indicates the time point at which supercritical water flushing was applied due to an overnight interruption.

dependent), which is associated with coking deactivation. SCW flushes partially reversed this coking (shown as dashed lines in Fig. 3a), but the catalyst quickly deactivated again. In contrast, applying the same SCW flush after sulfur-poisoning had no comparable effect (the second SCW flush between 5th and 6th H_2O_2 treatments). In each cycle, immediately after H_2O_2 treatment, the organic carbon conversion (X_{TOC}) was consistently lower than GEc, resulting in a carbon balance exceeding 100% (Fig. 3c). This excess suggests additional gasification of oxidized carbon support or residual coke from previous cycles. After seven cycles, the catalyst bed mass had decreased by 20%, indicating degradation of the carbon support and possible Ru loss. Such a loss is unlikely to result from handling, as catalyst recovery during loading and unloading is typically near quantitative. This structural degradation and material loss likely contributed to the observed performance decline.

To further investigate the decline in catalytic activity observed after several cycles, the spent catalyst after the 7-H_2O_2 experiment was characterized and compared to a fresh sample. The specific surface area decreased from 1021 m^2 g^{-1} to 336 m^2 g^{-1}, and the micropore volume dropped from 0.375 cm^3 g^{-1} to 0.129 cm^3 g^{-1}, while the mesopore volume only slightly decreased (from 0.062 cm^3 g^{-1} to 0.051 cm^3 g^{-1}), indicating that coke formation and the 7 cycles caused a loss of microporosity [7].

Since coke deposition is expected only during organic gasification, control experiments were performed to distinguish the effects of coke deposition from those of H_2O_2 treatment. Four samples were analysed (Fig. 4): (i) fresh Ru/AC, (ii) SCW treatment only, (iii) H_2O_2 treatment (100 °C) only, and (iv) H_2O_2 treatment (100 °C) followed by SCW. The fresh Ru/AC (i) exhibits a Type I(a) isotherm, characterized by a sharp N_2 uptake at low relative pressure ($P P_0^{-1} < 0.1$) followed by a plateau, with no apparent hysteresis, indicating a highly microporous material

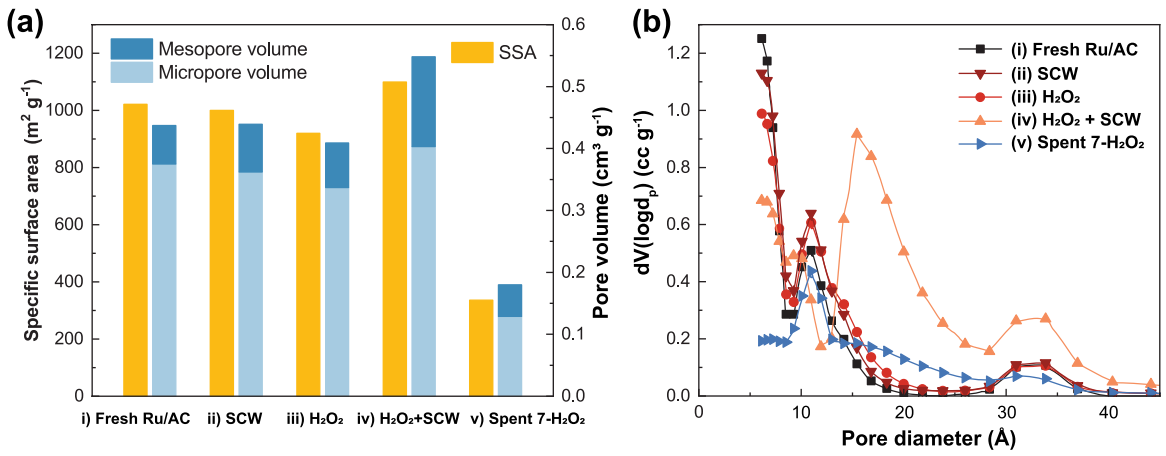

Fig. 4. (a) Specific surface area (SSA) and pore volume analysis of various Ru/AC samples by N_2 physisorption. (i) Fresh Ru/AC as received; (ii) Ru/AC treated with supercritical water (SCW) at 380 °C, 25 MPa for 2 h; (iii) Ru/AC treated with 3 wt% H_2O_2 at 100 °C, 25 MPa for 2 h; (iv) Ru/AC was subjected to two consecutive cycles of H_2O_2 (3 wt%, 100 °C, 25 MPa, 1 h) followed by SCW (380 °C, 25 MPa, 1 h) treatment; (v) spent 7-H_2O_2 catalyst after 7 cycles of deactivation-regeneration; (b) Pore size distribution of above-mentioned catalysts (shown up to 5 nm, as the curve flattens beyond this range; the full range of pore size distribution is in SI Fig. S10).

(Figure S9). In the absence of organic feed, SCW treatment alone (ii) preserved the carbon support structure, with minimal changes in pore size distribution compared to the fresh catalyst. H_2O_2 treated alone (iii) resulted in slightly reduced micropore volume and mild pore widening, consistent with a previous study [13]. In contrast, H_2O_2 treatment followed by SCW (iv), led to pronounced structural changes. The isotherm evolved from Type I(a) to Type I(b) (Figure S9): indicative of micropore widening and possibly narrow mesopore formation [61]. Specifically, the volume of micropores with diameters smaller than 9 Å decreased, while a significant fraction of transitional micro/mesopores emerged around 17 Å in diameter (Fig. 4b). The total pore volume increased from 0.437 $cm^3\ g^{-1}$ to 0.548 $cm^3\ g^{-1}$. These results suggest that activated carbon oxidized by H_2O_2 is prone to react with supercritical water to generate gases, creating new pores, enlarging micropores, and potentially causing crack formation, as reported previously [13].

In addition, inductively coupled plasma optical emission spectroscopy (ICP-OES) analysis of the spent 7-H_2O_2 catalyst revealed a residual sulfur content of 1193 ppm (mg S kg^{-1} catalyst), corresponding to approximately 14% of the sulfur content in the poisoned catalyst after a single poisoning cycle. These findings indicate that although this H_2O_2 regeneration is harsh enough to damage the carbon support, it is still insufficient for the complete sulfur removal. Overall, the performance decline observed after multiple H_2O_2 regeneration cycles is likely associated with a loss of active sites. Plausible contributors include:

(i) possible Ru loss associated with severe oxidation and partial gasification of the activated carbon support, which may lead to the formation of debris and detachment of Ru species;
(ii) reduced accessibility of Ru due to structural degradation;
(iii) accumulation of residual sulfur species, as evidenced by ICP, progressively building up over successive regeneration steps.

Therefore, further optimization is necessary to develop a regeneration strategy that effectively removes sulfur while preserving the activated carbon for repeated use.

To improve the regeneration protocol for sulfur removal and carbon support preservation, we monitored the stages at which sulfur and coke were largely removed by tracking the sulfur and carbon content in liquid effluent samples throughout the continuous regeneration process (Figure S16). The procedure involved an initial H_2O_2 treatment (85 °C), followed by temperature ramping from 85 °C to 400 °C using pure water, and concluded with an activity test using 20 wt% glycerol in water. Sulfur was primarily detected by ICP-OES in the effluent during the subcritical water phase (150 °C to 300 °C), indicating that this temperature ramping stage, situated between the H_2O_2 treatment and the activity test, plays a critical but previously overlooked role in effective regeneration. This suggests that sulfur species left after an H_2O_2 test are strongly adsorbed on the catalyst surface and cannot be efficiently washed away with H_2O_2 solution at 85 °C, requiring elevated temperatures for desorption.

Desorption of adsorbed species is generally a thermally activated process that follows Arrhenius-type behavior, with rate constants increasing exponentially with temperature [62]. Higher temperatures therefore accelerate desorption kinetics and can also shift the adsorption–desorption equilibrium toward desorption, as is commonly exploited in regenerating adsorbents [63]. However, once water becomes supercritical, solubility is the limiting factor: the dielectric constant of water drops sharply, reducing its polarity and thereby lowering the solubility of polar or ionic species [3]. As a result, the sulfur content in the effluent declines under supercritical conditions despite higher thermal energy.

These findings point to the oxidation and desorption happening in separate steps. During H_2O_2 treatment, sulfur is oxidized but does not immediately desorb because the temperature is too low to overcome its strong affinity for the catalyst surface. This affinity could be caused by electrostatic interactions, hydrogen bonding, van der Waals forces, entrapment, or covalent bonding such as with organosulfates (generally decomposing between 100 °C and 300 °C). Its delayed removal during the subsequent water flushing step likely hinders oxidation of the deeper sulfur layers, thereby preventing complete regeneration.

To prove whether the limited activity recovery is due to the incomplete sulfur removal, a second H_2O_2 treatment and water flush were introduced before the activity test, referred to as experiment 8-H_2O_2 (Fig. 5, first regeneration cycle), representing a two-step H_2O_2 regeneration. Each H_2O_2 step was followed by a subcritical water flush (temperature ramping from 100 °C to 374 °C over 40 min) and a supercritical water flush ($\geq$ 374 °C for 30 min). This two-step approach successfully restored catalytic activity, achieving full GEc recovery. Notably, sulfur was still detected in the process water during the second water flush (the sample taken at 300 °C water flushing contained 3.5 ppm sulfur). This may support the earlier hypothesis regarding the presence of underlying sulfur. Alternatively, it could indicate that the first subcritical water flush was insufficient to fully remove surface adsorbed sulfur.

To exclude the possibility of insufficient subcritical water flushing, a one-step H_2O_2 treatment in the second regeneration cycle in exp. 8-H_2O_2

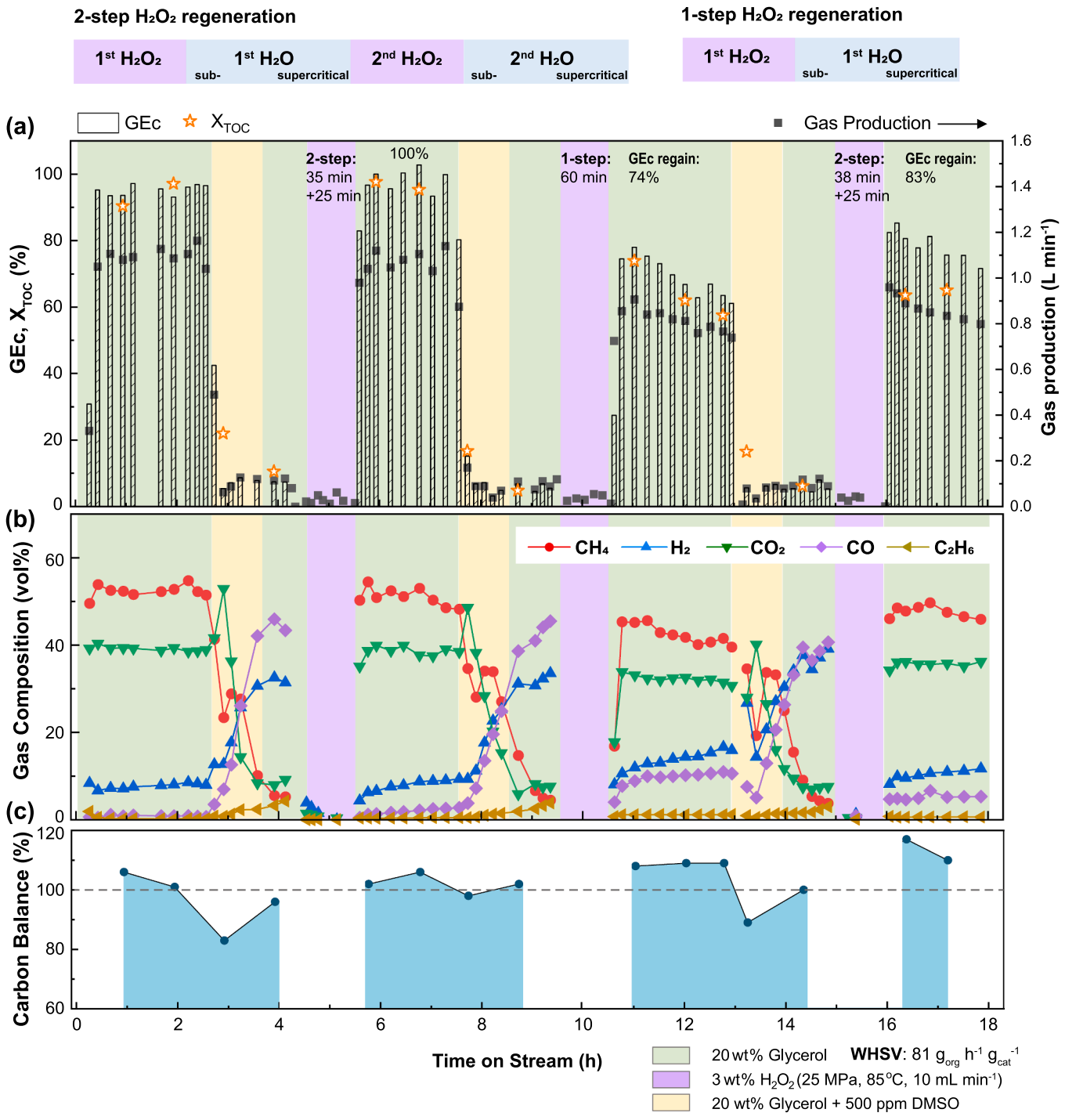

Fig. 5. 8-H_2O_2: Comparison of two-step and one-step H_2O_2 regeneration, with water flushing not considered as time on stream. (a) Gasification efficiency (GEc), organic carbon conversion (X_{TOC}), and gas production; (b) gas compositions obtained during the deactivation-regeneration-activity cycles; (c) the corresponding carbon balance. All hydrothermal gasification tests and poisoning were conducted at 400 °C and 25 MPa. X_{TOC} is organic carbon conversion based on total organic carbon (TOC) measured in the feed and effluent (Equation S3). Carbon balance (%) is calculated as the total carbon found in the gas and liquid phases divided by the carbon content of the feed (Equation S4). The drop in carbon balance during the sulfur poisoning step likely reflects the formation of carbonaceous deposits, while values exceeding 100% after regeneration may result from gasification of residual coke or partial degradation of the carbon support.

was conducted. The total H_2O_2 exposure time was kept constant, but the catalyst was held at subcritical water conditions (290 °C) for 50 min, until no sulfur was detected in the effluent, followed by 30 min under supercritical conditions. However, this method yielded only 74% GEc recovery, confirming that multiple H_2O_2 treatments are necessary to fully remove coke and sulfur blockages across accumulated layers. Furthermore, introducing organic feed before complete sulfur removal led to partial irreversible deactivation, likely because newly formed coke anchored residual sulfur more tightly to the catalyst [11]. This effect was observed in the third regeneration cycle of exp. 8-H_2O_2 and exp. 2-H_2O_2 (Figure S8), where subsequent H_2O_2 treatments proved less effective following an incomplete initial regeneration.

3.3. Optimization of the two-step H_2O_2 regeneration method

Given the effectiveness of the two-step H_2O_2 treatment, the next focus was placed on optimizing this regeneration approach. Since the catalytic activity of Ru/AC is closely linked to its textural properties (e.g., specific surface area, pore volume, and pore size distribution) and residual sulfur content, we used material characterization as a primary tool for rapid screening of regeneration conditions. To this end, a large batch of Ru/AC catalyst was deactivated using 20 wt% glycerol and 500 ppm DMSO (referred to as "S-Ru/AC") and subsequently divided into multiple 200 mg portions. These were tested under various conditions in a custom-built small flow reactor (system diagram shown in Figure S4). The tests examined the influence of H_2O_2 treatment temperature and duration, along with water flushing temperature, duration, and flow rate, as summarized in Table 1. Regeneration efficiency was assessed via ICP (for sulfur removal) and N_2 physisorption (for coke removal and preservation of pore structure). For clarity, each experimental condition is labeled as Regen-1, Regen-2, and so on.

ICP-OES analysis of the S-Ru/AC catalyst revealed an S content of approximately 8500 ± 500 mg kg^{-1}. Assuming sulfidation occurs only on the surface of Ru [5], and based on a 5 wt% Ru loading with around 50% dispersion estimated from TEM particle size (Figure S12), the calculated Ru_{surf}:S molar ratio is approximately 1:1. For comparison, Dreher et al. inferred by EXAFS a sulfur saturated phase of $RuS_{0.33}$ (Ru_{surf}:S ≈ 3:1) on Ru/C [5]. The higher sulfur content in our sample therefore suggests that a substantial fraction of sulfur is not bound to Ru but is instead incorporated into coke, both aromatic and aliphatic species, as shown in Fig. 1.

Among the two-step H_2O_2 regeneration protocols (Regen-4 to Regen-8), Regen-7 exhibited the highest sulfur removal efficiency, eliminating 97 ± 2% of the initial sulfur contamination. Interestingly, Regen-6, which achieved 94 ± 1% sulfur removal, differed from Regen-7 only in the use of a 10-minute supercritical water flush instead of an additional 10 min of subcritical water flushing. This comparison indicates that supercritical water flushing between the two H_2O_2 oxidation steps is not essential, and that subcritical water flushing plays a more critical role in facilitating sulfur removal. Both Regen-5 and Regen-8 showed comparable sulfur removal efficiencies (ca. 95%), indicating that higher temperatures applied for shorter durations can effectively remove sulfur. This also suggests that the second H_2O_2 oxidation step can be performed under milder conditions, as demonstrated by Regen-5. From an economic perspective, reducing H_2O_2 consumption, e.g., through shorter flushing times, is preferable. In contrast, Regen-4 achieved only 92 ± 1% sulfur removal, despite using a longer first oxidation duration. This result underscores that operating at a lower temperature (90 °C) is less effective, even with extended treatment time.

For comparison, a control experiment using one-step H_2O_2 regeneration (Regen-3) achieved 88% sulfur removal. This confirms that a two-step oxidation approach further improves sulfur removal efficiency compared to one-step regeneration. Interestingly, subcritical water flushing alone (Regen-2) removed 76% of sulfur, which is consistent with a previous report [40]. This may be attributed to partial oxidation of sulfur species upon exposure to air [64]. Indeed, the catalyst was first dried under flowing nitrogen prior to unloading and was subsequently exposed to air during unloading and reloading. In contrast, subcritical water flushing performed *in situ* immediately after sulfur poisoning does not recover the catalytic activity, supporting this assumption. Finally, H_2O_2 oxidation without any flushing (Regen-1) resulted in only 57% sulfur removal, highlighting that oxidation alone, without a high temperature flushing step, is not sufficient for effective regeneration.

Carbon support preservation after regeneration was evaluated using N_2 physisorption isotherm analysis. All regenerated catalysts (Regen-4–8) exhibited increased BET surface area (827–867 m^2 g^{-1}) and total pore volume (0.379–0.397 cm^3 g^{-1}) compared to the poisoned catalyst (758 m^2 g^{-1}, 0.344 cm^3 g^{-1}). In contrast, all the control experiments showed even lower specific surface area and total pore volume. Regen-1 showed a surface area and pore volume of 544 m^2 g^{-1} and 0.266 cm^3 g^{-1} which are lower than those before regeneration. This decrease may

Table 1
Optimization of conditions for the two-step H_2O_2 regeneration method (3 wt%), including H_2O_2 treatment temperature and duration, as well as water flushing temperature, duration, and flow rate in a specifically designed flow setup. SubC = subcritical water. Subcritical duration refers to the heating phase during which the temperature is ramped from 100 °C to 374 °C. SC = supercritical water. Supercritical duration refers to the isothermal holding period at temperatures ranging from 375 °C to 385 °C, above the critical point.

Test code	1st H_2O_2 oxidation (3 mL min^{-1})	1st Water flush (4 mL min^{-1})		2nd H_2O_2 oxidation (3 mL min^{-1})	2nd Water flush (4 mL min^{-1})		S content (mg kg^{-1})[e]	Sulfur removal (%)	BET SSA (m^2 g^{-1})	V_{total} (cm^3 g^{-1})	$V_{microp.}$[c] (cm^3 g^{-1})
		SubC (min)	SC (min)		SubC (min)	SC (min)					
Fresh Ru/AC	N/A	N/A		N/A	N/A		<[b]	-	1021	0.437	0.375
S-Ru/AC[a]	N/A	N/A		N/A	N/A		8500 ± 500	-	758	0.344	0.271
Regen-1	100 °C 26 min	N/A		N/A	N/A		3700	57	544	0.266	0.186
Regen-2	N/A	47	0	N/A	N/A		2000	76	654	0.315	0.225
Regen-3	100 °C 13 min	52	0	N/A	N/A		1000	88	664	0.319	0.230
Regen-4	90 °C 20 min	47	10	90 °C 13 min	47	10	740 ± 120	92 ± 1	829	0.385	0.294
Regen-5	100 °C 13 min	51	10	80 °C 5 min	50	10	430 ± 40	95 ± 0	840	0.383	0.300
Regen-6	100 °C 13 min	45	10	100 °C 13 min	40	10	580 ± 120	94 ± 1	827	0.383	0.295
Regen-7	100 °C 13 min	55	0	100 °C 13 min	50	0	290 ± 130	97 ± 2	867	0.397	0.310
Regen-8	120 °C 5 min	45[d]	10[d]	100 °C 5 min	31[d]	10[d]	510 ± 120	95 ± 1	828	0.379	0.296

[a] Sulfur poisoning of Ru/AC was achieved by feeding 20 wt% glycerol with 500 ppm DMSO for 1.5 h, followed by an additional 1.5 h of 20 wt% glycerol. GEc decreased from over 99% (CH_4: 56.0%; H_2: 4.0%; CO_2: 40.0%; CO: 0.4%) to less than 15% (CH_4: 4.0%; H_2: 29.0%; CO_2: 9.0%; CO: 46.0%; C_2H_6: 5.6%) after poisoning.
[b] < : below detection limit (0.02 ppm in solution, equivalent to around 20 ppm sulfur on solid sample)
[c] The total pore volume was measured at P P_0^{-1} ≥ 0.99, and the micropore volume was determined using the t-plot method.
[d] The water flushing flow rate in Regen-8 is 8 mL min^{-1}.
[e] The error margins for sulfur removal are derived from two independent sample analyses; values reported without error margins are based on a single analysis.

result from oxidation of sulfur and carbon to free adsorbed species which may have migrated into the micropores and caused pore blockage. Regen-2 and Regen-3 exhibited improved microporosity (c.a. 660 m^2 g^{-1}, 0.320 cm^3 g^{-1}) relative to Regen-1, likely due to flushing of these free adsorbed species, yet their values remained below those of the untreated poisoned sample. These results indicate that subcritical water flushing alone or one-step H_2O_2 regeneration is insufficient to fully restore the porous structure, and the decrease of surface area and pore volume could be due to incomplete removal of oxidized sulfur and carbon species.

Although the two-step regenerated samples still exhibited lower surface area and pore volumes than the fresh material (1021 m^2 g^{-1}, 0.437 cm^3 g^{-1}), the observed decrease in micropore volume together with an increase in mesopore volume indicates varying degrees of H_2O_2-induced pore widening. Nonetheless, the loss in surface area and microporosity was kept within 20% through the optimized regeneration protocol. Among the tested conditions, Regen-7 achieved the highest sulfur removal efficiency (97 ± 2%) and the largest micropore volume (0.310 cm^3 g^{-1}), demonstrating that subcritical water flushing is more effective than supercritical water in removing oxidized sulfur, while avoiding supercritical conditions after oxidative treatment also preserves microporosity and minimizes damage to carbon support. Regen-7 therefore represents the most effective regeneration strategy, balancing sulfur removal and porosity regain with structural preservation, with only minor mesopore development.

3.4. *Ex situ XPS analysis of catalyst surface sulfur species*

X-ray photoelectron spectroscopy (XPS) was employed to investigate the evolution of surface sulfur species on Ru/AC during sulfur poisoning and subsequent regeneration (Fig. 6). It should be noted that all XPS measurements were conducted ex situ; therefore, partial oxidation of surface species during air exposure prior to analysis cannot be excluded [64]. As a result, the measured sulfur oxidation states do not necessarily reflect the exact in situ chemical states during cHTG operation. The XPS results provide qualitative, surface-sensitive evidence for sulfur presence and removal, complementing bulk sulfur quantification by ICP-OES.

No detectable S 2p signal was observed for the fresh Ru/AC catalyst. After sulfur poisoning (Fig. 6d), a pronounced S 2p doublet centered at approximately 168.4 eV appeared, which is characteristic of oxidized sulfur species (S(VI)), such as sulfate, sulfonate, and organosulfate [65,66]. The predominance of these oxidized sulfur species is likely associated with oxidation of sulfur-containing surface species upon exposure to air after reactor operation. In addition, a weak signal at lower binding energies (163–164 eV) was detectable, which may be associated with organic sulfur species (e.g., C-S-H/C-S-C) [66,67]. However, due to its low intensity and proximity to the noise level, this contribution was not further deconvoluted.

Following H_2O_2 treatment (Fig. 6c) or subcritical water flushing (Fig. 6b), the S 2p signal associated with oxidized sulfur species remained detectable but with reduced intensity, corresponding to approximately 44% and 26% of the surface sulfur remaining relative to the sulfur-poisoned catalyst (S-Ru/AC), respectively. This trend is consistent with the residual sulfur concentrations quantified by ICP-OES, which also indicate sulfur retentions of 44% and 24%, respectively. In contrast, no measurable S 2p signal was detected for the fully regenerated catalyst (Fig. 6a), indicating effective removal of sulfur species from the catalyst surface.

The XPS survey and O 1 s and Ru 3p spectra are listed in supporting information Section 7.3.

3.5. *Monitoring sulfur and coke leaching during regeneration*

During the experiments from Regen-1 to Regen-8, temperature and conductivity were also monitored *in situ*, and leached carbon and sulfur

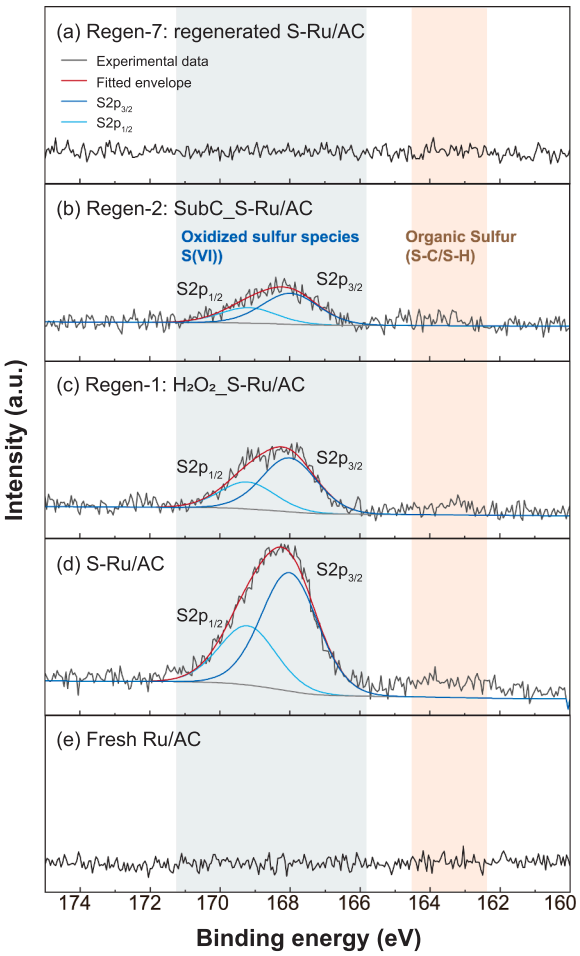

Fig. 6. S 2p XPS spectra of Ru/AC catalysts at different stages of sulfur poisoning and regeneration: (a) Regen-7: regenerated S-Ru/AC, (b) Regen-2: subcritical water treated S-Ru/AC, (c) Regen-1: H_2O_2-treated S-Ru/AC, (d) S-Ru/AC: sulfur-poisoned Ru/AC, and (e) fresh Ru/AC. The S 2p spectra were deconvoluted into S $2p_{3/2}$ and S $2p_{1/2}$ spin-orbit doublets using a fixed area ratio of 2:1 and a spin-orbit splitting of 1.2 eV. The grey shaded region highlights the binding energy range centered at 168–169 eV, which is characteristic of highly oxidized sulfur species (S(VI)), including sulfate, sulfonate, and organosulfate. Minor contributions at lower binding energies, highlighted in orange (centered at 163–164 eV), are attributed to reduced or organic sulfur species (e.g., C–S–H or C–S–C species).

contents measured *ex situ* (Fig. 7). The H_2O_2 treatment began with a heating phase using water as the feed. Once the target temperature was reached and stabilized, the feed was switched to H_2O_2. This switch resulted in a sharp increase in conductivity, followed by a decline, with peak conductivity varying depending on temperature (Figure S17). In the subsequent water flushing phase, the temperature was increased stepwise, revealing three distinct conductivity peaks at approximately 180 °C, 250 °C, and 320 °C (Figure 7b, f).

To evaluate the impact of sulfate on conductivity and assess the use of conductivity measurement to track sulfur release, total sulfur content and sulfate contents were measured offline and compared to conductivity values. During the water flushing phase, conductivity showed a strong linear correlation with total sulfur content measured by ICP-OES ($R^2 = 0.9999$, Figure S1), and total sulfur was equal to the sulfate sulfur, suggesting that sulfate is the sole sulfur species present at this stage. This indicates that the observed conductivity peaks correspond directly to sulfate desorption occurring under subcritical water conditions. In this case, integrating the conductivity curve provides a reliable estimate of the sulfur removal amount. For example, integration of the conductivity

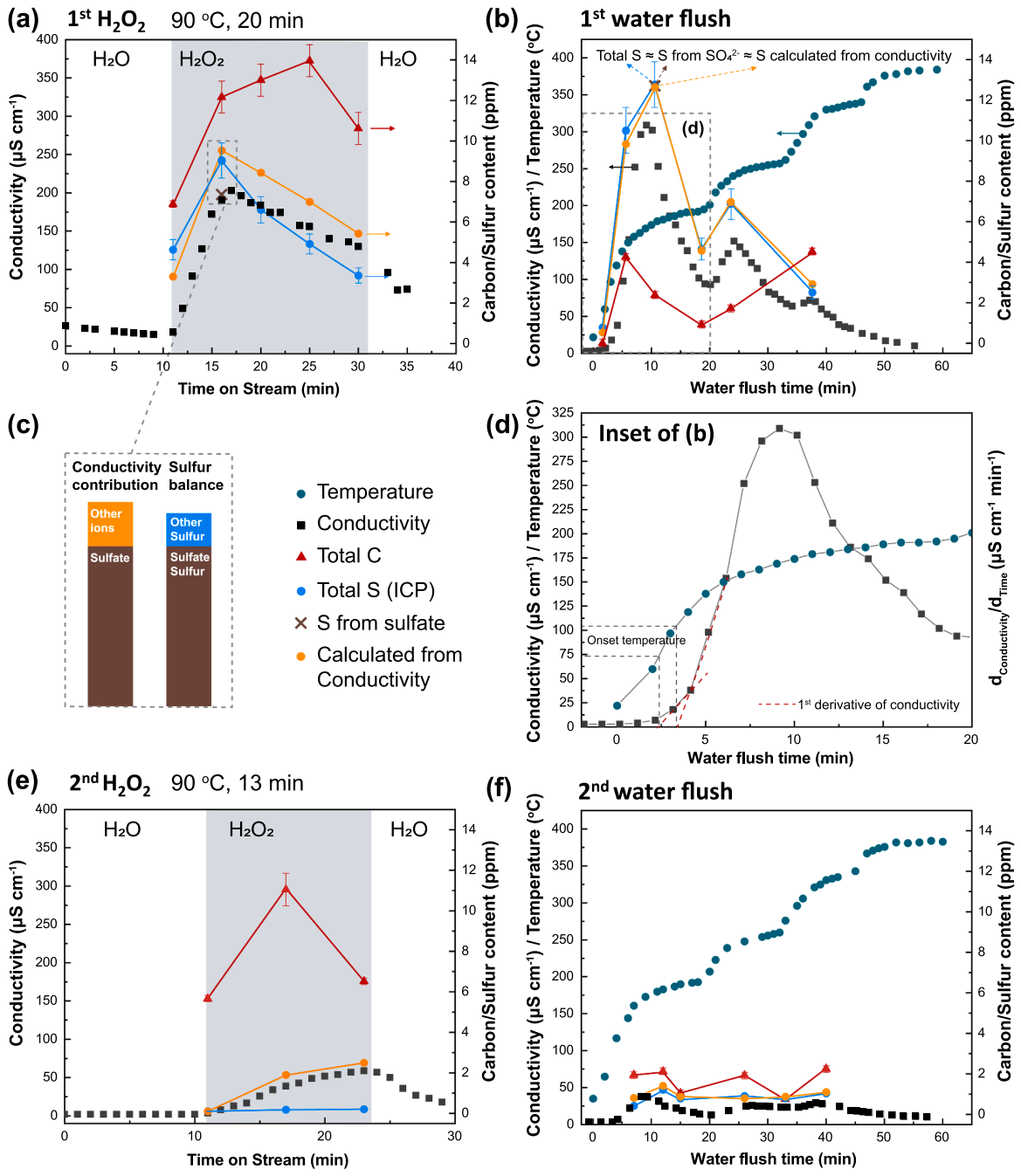

Fig. 7. Regen-4: Conductivity and temperature recordings during 1st (a) and 2nd (e) H_2O_2 treatment and 1st (b) and 2nd (f) water flushing, along with analytical data including carbon content and sulfur content from various methods. (c) is the inset of (a), illustrating the balance of ionic and sulfur species. (d) is the inset of (b), indicating the onset temperature for sulfate desorption (75–105 °C). The conductivity probe is located at the outlet of the setup, while the temperature sensor is positioned at the catalyst bed of the reactor. The residence time delay (lag time) between the reactor and outlet has been corrected using data from an experiment with a tracer. Error bars represent the standard deviation of repeated analytical measurements.

signal in the control experiment Regen-2 indicates 72% sulfur removal, close to the 76% determined by ICP-OES, validating the use of conductivity as a quantitative proxy for sulfate removal. In contrast, during the H_2O_2 treatment phase, discrepancies were observed among total sulfur, sulfate sulfur, and conductivity-derived sulfur (based on the conductivity–sulfur correlation). For example, in Fig. 7c (corresponding to the dashed box of Fig. 7a), the conductivity-derived value is the highest, as conductivity reflects all ionic species, indicating the presence of potential partially oxidized sulfur intermediates and ionic carbon species, e.g., carboxylates. Additionally, total sulfur content exceeds sulfate-sourced sulfur, suggesting the possible presence of organosulfur compounds or partially oxidized sulfur intermediates. Thus, during H_2O_2 treatment, conductivity can qualitatively indicate contaminant leaching but cannot precisely quantify sulfur content.

Carbon (coke) removal occurred primarily during the H_2O_2 oxidation phases, as evidenced by the release of carbon detected during both the first and second H_2O_2 treatments (Fig. 7a, e). Sulfur species were leached during both the H_2O_2 and water flushing phases. During the subcritical water flush, sulfate desorption exhibited a temperature-dependent profile, with an onset threshold between 75 °C and 105 °C and a maximum between 150 °C and 180 °C. At temperature plateaus, conductivity peaks declined but rose again with further temperature

increases, suggesting a broad variety of adsorption sites with different adsorption strengths, and/or different organosulfates of different thermal stability. The pH values of the effluent were consistently between 3 and 4 in both H_2O_2 and water flushing steps (Figure S18-19) and varied only slightly with sulfate concentration. For reference, dilute sulfuric acid solutions in the low-ppm range give pH values in this interval, consistent with the acid dissociation constants of sulfuric acid ($pK_{a1} \approx -3$, $pK_{a2} \approx 2$), indicating that the desorbed species are present predominantly as sulfate (SO_4^{2-}) with only a minor fraction as bisulfate (HSO_4^-).

The tracking of leached sulfur and carbon in the control experiments (Regen 1–3) is shown in Fig. 8. Unlike the subcritical water flushing steps in Regen-4 to Regen-8, Regen-2 showed a mismatch between total sulfur, sulfate sulfur, and conductivity-derived sulfur, indicating that the desorbed sulfur species were not solely sulfate. This discrepancy likely reflects incomplete oxidation during air exposure in the absence of preceding H_2O_2 treatment. In comparison, Regen-3, which included an H_2O_2 oxidation step prior to subcritical water flushing, showed no difference between sulfate and total sulfur and shifted the sulfate desorption peak temperature from 220 °C (observed in Regen-2) to 190 °C. This demonstrates that the H_2O_2 oxidation step promotes the oxidation of sulfur species remaining after the poisoning and air exposure into sulfate, and/or that the H_2O_2 treatment impacted the strength of the adsorption sites. These results reinforce the complementary roles of H_2O_2 oxidation (for coke removal and sulfur oxidation) and subcritical water flushing (for thermally driven sulfate desorption), highlighting the necessity of combining both steps for effective catalyst regeneration.

Based on the conductivity evolution with temperature and the inferred species, a phenomenological mechanism is proposed and illustrated in Fig. 9. During the first H_2O_2 treatment (Fig. 9a), Ru is

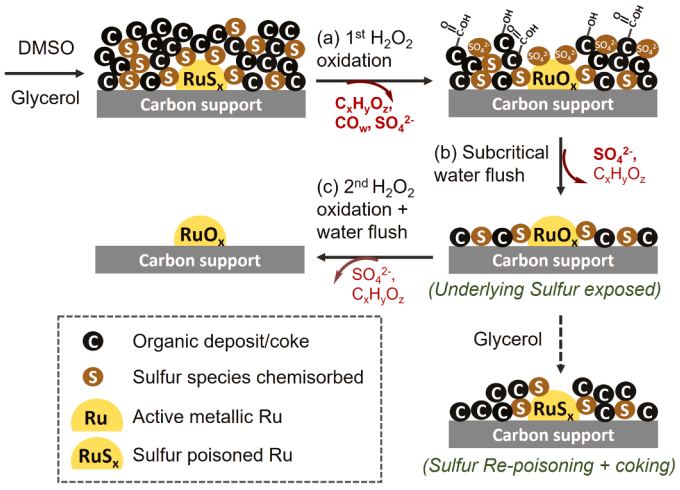

Fig. 9. Schematic diagram illustrating the proposed phenomenological mechanism of H_2O_2-water flushing regeneration.

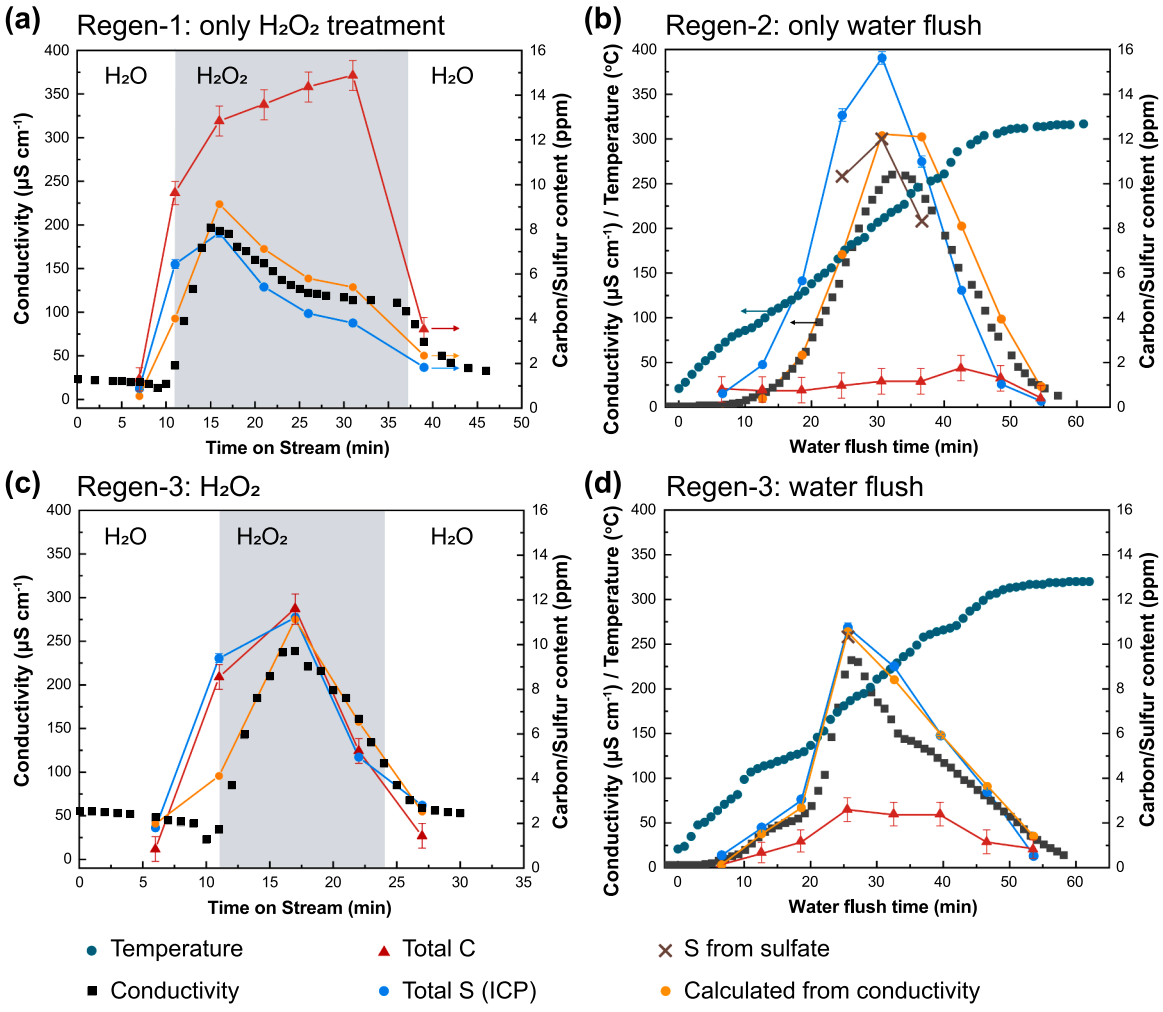

Fig. 8. Control experiments. (a) Regen-1: only H_2O_2 treatment (100 °C). (b) Regen-2: only subcritical water flushing. (c-d) Regen-3: one-step H_2O_2 (100 °C) regeneration. Error bars represent the standard deviation of repeated analytical measurements.

oxidized, as previously reported [13], while surface and near-surface coke and sulfur species are also oxidized, forming CO and CO_2 (detected by GC) and organic compounds that are flushed away and detected as TOC. In this step, sulfur is only partially removed, mainly as sulfate. However, some oxidized sulfur is presumed to remain strongly adsorbed, inhibiting further oxidation of deeper sulfur and coke layers. The removal of these oxidized species is thermally driven, particularly for sulfate, which exhibits a temperature-dependent desorption profile during the subsequent subcritical water flushing (Fig. 9b). It also helps expose deeper sulfur-rich layers for further oxidation, enabling more complete regeneration. In the second H_2O_2 treatment (Fig. 9c), these newly exposed sulfur species and any residual coke are efficiently oxidized, further cleaning the catalyst surface, as evidenced by the continued detection of sulfur species in the second water flush (Fig. 7). Upon re-exposure to organic feed, RuO_2 is reduced back to metallic Ru above 125 °C [5], completing the regeneration cycle. However, if the second H_2O_2 step is omitted, sulfates remaining on the catalyst surface can lead to partial resulfidation of Ru during the subsequent glycerol test and limit the recovery of GEc.

4. Conclusions

From this study, we conclude that effective regeneration of sulfur- and coke-deactivated Ru/AC catalysts requires complementary roles of oxidation and desorption steps. Treatments relying on only one of these steps are insufficient: without prior wet oxidation, sulfur species remain less or non-desorbable and coke deposits persist; without a desorption step, 30–40% of (oxidized) sulfur species remain strongly adsorbed on the catalyst surface, preventing complete removal of sulfur and coke contaminants. The high sulfur removal efficiency and preservation of activated carbon microporosity achieved with the two-step H_2O_2–subcritical water flushing method demonstrate that liquid-phase oxidative regeneration is a viable strategy for sulfur-poisoned Ru/AC catalysts. From a techno-economic and operational perspective, in situ aqueous regeneration strategies are compatible with continuous catalytic hydrothermal gasification, as catalyst replacement, regeneration in the gas phase or ex situ regeneration would typically entail significant downtime, higher operating costs, and increased capital expenditure (CAPEX). These insights have broader implications for the regeneration of metal-on-carbon catalysts used in other applications, such as hydrothermal liquefaction (HTL) or aqueous-phase reforming (APR), where sulfur- and coke-related deactivation is also a major challenge. Applying a sequential oxidation–desorption strategy could therefore extend catalyst lifetime and improve process efficiency in such systems.

CRediT authorship contribution statement

David Baudouin: Writing – review & editing, Writing – original draft, Project administration, Methodology. **Frédéric Vogel:** Writing – review & editing, Supervision, Funding acquisition, Conceptualization. **Weicheng Hua:** Writing – review & editing, Investigation. **Saša Bjelić:** Writing – review & editing, Writing – original draft, Methodology. **Songlan Sun:** Writing – review & editing, Writing – original draft, Methodology, Investigation.

Declaration of Competing Interest

The authors declare that they have no known competing financial interests or personal relationships that could have appeared to influence the work reported in this paper.

Acknowledgment

The authors gratefully acknowledge Thomas Brunner for designing and building the regeneration setup, assisting with the cHTG experiments, and drafting the setup description; Inge Stockinger for ICP-OES training and analysis; Mario El Kazzi for providing access to XPS instrumentation and for valuable discussions on data analysis; Amel Tumbul for upgrading the continuous gasification setup; Daniel Fischer for assistance with the cHTG experiments; Xujun Li for help with installing the regeneration setup; Dmitrii Sharkov for DIMATOC training; and Dmitrii Komissarenko for conducting preliminary experiments. Part of this work was supported by and performed within the Energy System Integration Platform at the Paul Scherrer Institute. The authors also thank TreaTech for providing the industrially deactivated, and acrylic acid deactivated Ru/AC catalysts. This project was funded by Innosuisse, grant number 56474.1 IP-EE.

Appendix A. Supporting information

Supplementary data associated with this article can be found in the online version at doi:10.1016/j.supflu.2026.106970.

Data availability

Data will be made available on request.

References

[1] F. Lin, M. Xu, K.K. Ramasamy, Z. Li, J.L. Klinger, J.A. Schaidle, et al., Catalyst deactivation and its mitigation during catalytic conversions of biomass, ACS Catal. 12 (2022) 13555–13599, https://doi.org/10.1021/acscatal.2c02074.
[2] J.P. Lange, Renewable feedstocks: the problem of catalyst deactivation and its mitigation, Angew. Chem. Int. Ed. 54 (2015) 13187–13197, https://doi.org/10.1002/anie.201503595.
[3] F. Vogel, Catalytic conversion of high-moisture biomass to synthetic natural gas in supercritical water. Handbook of Green Chemistry, Wiley, 2010, pp. 281–324, https://doi.org/10.1002/9783527628698.hgc024.
[4] C. Hunston, D. Baudouin, M. Tarik, O. Kröcher, F. Vogel, Investigating active phase loss from supported ruthenium catalysts during supercritical water gasification, Catal. Sci. Technol. 11 (2021) 7431–7444, https://doi.org/10.1039/d1cy00379h.
[5] M. Dreher, B. Johnson, A.A. Peterson, M. Nachtegaal, J. Wambach, F. Vogel, Catalysis in supercritical water: pathway of the methanation reaction and sulfur poisoning over a Ru/C catalyst during the reforming of biomolecules, J. Catal. 301 (2013) 38–45, https://doi.org/10.1016/j.jcat.2013.01.018.
[6] T. Yeh, S. Linic, P.E. Savage, Deactivation of pt catalysts during hydrothermal decarboxylation of butyric acid, ACS Sustain Chem. Eng. 2 (2014) 2399–2406, https://doi.org/10.1021/sc500423b.
[7] G. Peng, M. Steib, F. Gramm, C. Ludwig, F. Vogel, Synthesis factors affecting the catalytic performance and stability of Ru/C catalysts for supercritical water gasification, Catal. Sci. Technol. 4 (2014) 3329–3339, https://doi.org/10.1039/c4cy00586d.
[8] D.C. Elliott, M.R. Phelps, L.J. Sealock, E.G. Baker, Chemical processing in high-pressure aqueous environments. 4. Continuous-flow reactor process development experiments for organics destruction 33 (1994).
[9] Elliott D.C., Sealock L.J., Baker E.G. Kinetics, Catalysis, and Reaction Engineering Chemical Processing in High-Pressure Aqueous Environments. 2. Development of Catalysts for Gasification. vol. 32. 1993.
[10] M. Osada, O. Sato, K. Arai, M. Shirai, Stability of supported ruthenium catalysts for lignin gasification in supercritical water, Energy Fuels 20 (2006) 2337–2343, https://doi.org/10.1021/ef060356h.
[11] M.H. Waldner, F. Krumeich, F. Vogel, Synthetic natural gas by hydrothermal gasification of biomass, J. Supercrit. Fluids 43 (2007) 91–105, https://doi.org/10.1016/j.supflu.2007.04.004.
[12] J.N. Jocz, P.E. Savage, L.T. Thompson, Thermodynamic analysis of catalyst stability in hydrothermal reaction media, Ind. Eng. Chem. Res 57 (2018) 8655–8663, https://doi.org/10.1021/acs.iecr.8b01334.
[13] M. Dreher, M. Steib, M. Nachtegaal, J. Wambach, F. Vogel, On-stream regeneration of a sulfur-poisoned ruthenium-carbon catalyst under hydrothermal gasification conditions, ChemCatChem 6 (2014) 626–633, https://doi.org/10.1002/cctc.201300791.
[14] A.R. Katritzky, D.A. Nichols, M. Siskin, R. Murugan, M. Balasubramanian, Reactions in high-temperature aqueous media, Chem. Rev. 101 (2001) 837–892, https://doi.org/10.1021/cr960103t.
[15] D. Salionov, C. Hunston, F. Vogel, D. Baudouin, S. Bjelić, The nature of carbon deposits and their formation pathways during catalytic supercritical water gasification of glycerol, J. Catal. 426 (2023) 257–269, https://doi.org/10.1016/j.jcat.2023.07.003.
[16] D. Baudouin, H. Xiang, F. Vogel, On the selective desulphurization of biomass derivatives in supercritical water, Biomass. Bioenergy 164 (2022) 106529, https://doi.org/10.1016/j.biombioe.2022.106529.
[17] J. Wambach, M. Schubert, M. Döbeli, F. Vogel, Characterization of a spent Ru/C catalyst after gasification of biomass in supercritical water. Chimia (Aarau), Swiss Chemical Society, 2012, pp. 706–711, 6610.2533/chimia.2012.706.

[18] Zöhrer H. Hydrothermal Gasification of Fermentation Residues for SNG-Production. PhD thesis 21316. ETH Zürich, 2013.
[19] C. Chang, F. Vogel, O. Kröcher, D. Baudouin, The effect of Ni- and Mo-based materials on thermochemical sulfate reduction by glycerol under hydrothermal process conditions, Chem. Eng. Res. Des. 205 (2024) 459–466, https://doi.org/10.1016/j.cherd.2024.03.024.
[20] T. Voisin, A. Erriguible, D. Ballenghien, D. Mateos, A. Kunegel, F. Cansell, et al., Solubility of inorganic salts in sub- and supercritical hydrothermal environment: application to SCWO processes, J. Supercrit. Fluids 120 (2017) 18–31, https://doi.org/10.1016/j.supflu.2016.09.020.
[21] Cheng Chang. Behavior of Sulfur under Hydrothermal Conditions: Removal Strategies for Catalytic Processes. PhD thesis 10715. EPFL, 2024.
[22] D.C. Elliott, T.R. Hart, A.J. Schmidt, G.G. Neuenschwander, L.J. Rotness, M. V. Olarte, et al., Process development for hydrothermal liquefaction of algae feedstocks in a continuous-flow reactor, Algal Res. 2 (2013) 445–454, https://doi.org/10.1016/j.algal.2013.08.005.
[23] G. Peng, C. Ludwig, F. Vogel, Catalytic supercritical water gasification: interaction of sulfur with ZnO and the ruthenium catalyst, Appl. Catal. B 202 (2017) 262–268, https://doi.org/10.1016/j.apcatb.2016.09.011.
[24] G. Peng, F. Vogel, D. Refardt, C. Ludwig, Catalytic supercritical water gasification: continuous methanization of chlorella vulgaris, Ind. Eng. Chem. Res 56 (2017) 6256–6265, https://doi.org/10.1021/acs.iecr.7b00042.
[25] H. Xiang, D. Baudouin, F. Vogel, Metal oxide nanoparticles embedded in porous carbon for sulfur absorption under hydrothermal conditions, Sci. Rep. 13 (2023) 9987, https://doi.org/10.1038/s41598-023-36395-8.
[26] J. Zhou, J. Zhao, J. Zhang, T. Zhang, M. Ye, Z. Liu, Regeneration of catalysts deactivated by coke deposition: a review, Chin. J. Catal. 41 (2020) 1048–1061, https://doi.org/10.1016/S1872-2067(20)63552-5.
[27] C.A. Querini, Isobutane/butene alkylation: regeneration of solid acid catalysts, Catal. Today 62 (2000) 135–143, https://doi.org/10.1016/S0920-5861(00)00415-6.
[28] F. Talebkeikhah, S. Sun, J.S. Luterbacher, Sinter-resistant nickel catalyst for lignin hydrogenolysis achieved by liquid phase atomic layer deposition of alumina, Adv. Energy Mater. 13 (2023), https://doi.org/10.1002/aenm.202203377.
[29] W. Lan, Y.P. Du, S. Sun, J. Behaghel De Bueren, F. Héroguel, J.S. Luterbacher, Continuous hydrogenolysis of acetal-stabilized lignin in flow, Green Chem. 23 (2021) 320–327, https://doi.org/10.1039/d0gc02928a.
[30] H.A. Abdullah, A. Hauser, F.A. Ali, A. Al-Adwani, Optimal conditions for coke extraction of spent catalyst by accelerated solvent extraction compared to Soxhlet, Energy Fuels 20 (2006) 320–323, https://doi.org/10.1021/ef050227l.
[31] Bjelić S., Gasser U., Alxneit I., Vogel F. Deactivation of Methanation Catalyst (Ru / C) Under Supercritical Water by Deposition of Non-Volatile Organics: First Insights Into Deposition Patterns and Chemical Properties 2019:1747–55. ⟨https://doi.org/10.1002/cctc.201801615⟩.
[32] I.V. Kozhevnikov, S. Holmes, M.R.H. Siddiqui, Coking and regeneration of H3PW12O40/SiO2 catalysts, Appl. Catal. A Gen. 214 (2001) 47–58, https://doi.org/10.1016/S0926-860X(01)00469-0.
[33] F.M. Gumerov, A.A. Sagdeev, R.F. Gallyamov, A.T. Galimova, K.A. Sagdeev, Regeneration of the catalysts by supercritical fluid extraction, Int. J. Anal. Mass Spectrom. Cromatogr. 02 (2014) 1–14, https://doi.org/10.4236/ijamsc.2014.21001.
[34] D. Kuzmenko, A.H. Clark, T. Schildhauer, J. Szlachetko, M. Nachtegaal, Operando sulfur speciation during sulfur poisoning-regeneration of Ru/SiO2 and Ru/Al2O3 using non-resonant sulfur Kα1,2 emission, RSC Adv. 10 (2020) 15853–15859, https://doi.org/10.1039/d0ra03068f.
[35] L.J. Hoyos, M. Primet, H. Praliaud, Sulfur poisoning and regeneration of palladium based catalysts, J. Chem. Soc. 88 (1992) 3367–3373, https://doi.org/10.1039/FT9928803367i.
[36] C. Fang, M.P. Harold, Low temperature NH3 regeneration of a sulfur poisoned Pt/Al2O3 monolith catalyst, Catal. Sci. Technol. 13 (2023) 6718–6732, https://doi.org/10.1039/d3cy01153d.
[37] A.A. Galkin, V.V. Lunin, Subcritical and supercritical water: a universal medium for chemical reactions, Usp. Khim 74 (2005) 24–40, https://doi.org/10.1070/rc2005v074n01abeh001167.
[38] Y. Cheng, F. Xue, S. Yu, S. Du, Y. Yang, Subcritical water extraction of natural products, Molecules 26 (2021) 4004, https://doi.org/10.3390/molecules26134004.
[39] Shvedov D., Tremaine P.R. The Solubility of Sodium Sulfate and the Reduction of Aqueous Sulfate by Magnetite under Near-Critical Conditions †. vol. 29. 2000.
[40] M. Osada, N. Hiyoshi, O. Sato, K. Arai, M. Shirai, Subcritical water regeneration of supported ruthenium catalyst poisoned by sulfur, Energy Fuels 22 (2008) 845–849, https://doi.org/10.1021/ef7005194.
[41] L. Zhao, S. Yang, J. Duan, Q. Liu, Improved NO reduction in the presence of SO2 by using Zr-promoted calcined NiAl hydrotalcite-like compounds and the regeneration of deactivated catalysts, Fuel 263 (2020) 116668, https://doi.org/10.1016/j.fuel.2019.116668.
[42] X. Ren, Z. Ou, B. Wu, Low-temperature selective catalytic reduction DeNOX and regeneration of Mn–Cu catalyst supported by activated coke, Materials 14 (2021) 5958, https://doi.org/10.3390/ma14205958.
[43] J. Ftouni, H.C. Genuino, A. Muñoz-Murillo, P.C.A. Bruijnincx, B.M. Weckhuysen, Influence of sulfuric acid on the performance of Ruthenium-based catalysts in the liquid-phase hydrogenation of Levulinic acid to γ-Valerolactone, ChemSusChem 10 (2017) 2891–2896, https://doi.org/10.1002/cssc.201700768.
[44] Z. Sheng, Y. Hu, J. Xue, X. Wang, W. Liao, SO2 poisoning and regeneration of Mn-Ce/TiO2 catalyst for low temperature NOx reduction with NH3, J. Rare Earths 30 (2012) 676–682, https://doi.org/10.1016/S1002-0721(12)60111-2.
[45] M.R. Hoffmann, Kinetics and mechanism of oxidation of hydrogen sulfide by hydrogen peroxide in acidic solution, Environ. Sci. Technol. 11 (1977) 61–66, https://doi.org/10.1021/es60124a004.
[46] S. Bjelić, U. Gasser, I. Alxneit, F. Vogel, Deactivation of methanation catalyst (Ru/C) under supercritical water by deposition of non-volatile organics: first insights into deposition patterns and chemical properties, ChemCatChem 11 (2019) 1747–1755, https://doi.org/10.1002/cctc.201801615.
[47] H. Zöhrer, F. Mayr, F. Vogel, Stability and performance of ruthenium catalysts based on refractory oxide supports in supercritical water conditions, Energy Fuels 27 (2013) 4739–4747, https://doi.org/10.1021/ef400707f.
[48] N. Ghaloum, S. Ok, Solid-state ^{13}C NMR analysis of regenerated and coked catalyst under dry and wet hydrotreatment, React. Kinet. Mech. Catal. (2025), https://doi.org/10.1007/s11144-025-02905-0.
[49] P. Guerra, A. Zaker, P. Duan, A.R. Maag, G.A. Tompsett, A.B. Brown, et al., Analysis of coke formed during zeolite-catalyzed supercritical dodecane cracking: Effect of supercritical water, Appl. Catal. A Gen. 590 (2020) 117330, https://doi.org/10.1016/j.apcata.2019.117330.
[50] Con-Yan Chen. US6632765, 2000.
[51] T.C. Tsai, Reactivation of acidic sites in mordenite used in toluene disproportionation, Appl. Catal. A Gen. 301 (2006) 292–298, https://doi.org/10.1016/j.apcata.2005.12.011.
[52] P.T.H. Pham, C.Q. Pham, T.-T. Dam, Q.-A. Nguyen, T.M. Nguyen, A comprehensive review of catalyst deactivation and regeneration in heavy oil hydroprocessing, Fuel Process. Technol. 267 (2025) 108170, https://doi.org/10.1016/j.fuproc.2024.108170.
[53] E. Truszkiewicz, A. Bielecka, E.M. Iwanek, M. Ojrzyńska, A. Ostrowski, CO Removal from hydrogen stream through methanation on Ru/C catalysts doped with Lanthanum and Barium, Hydrogen 4 (2023) 389–407, https://doi.org/10.3390/hydrogen4020027.
[54] H.S. Zeng, T. Hihara, K. Inazu, K. Aika, Effect of methanation of active carbon support on the barium-promoted ruthenium catalyst for ammonia synthesis, Catal. Lett. 76 (2001) 193–199, https://doi.org/10.1023/A:1012201613791.
[55] Teixeira Da Silva V.L.S., Lima F.P., Dieguez L.C., Schmal M. Regeneration of a Deactivated Hydrotreating Catalyst. 1998.
[56] S.K. Bhargava, J. Tardio, J. Prasad, K. Föger, D.B. Akolekar, S.C. Grocott, Wet oxidation and catalytic wet oxidation, Ind. Eng. Chem. Res. 45 (2006) 1221–1258, https://doi.org/10.1021/ie051059n.
[57] T. Yokoyama, Y. Matsumoto, G. Meshitsuka, Enhancement of the reaction between pulp components and hydroxyl radical produced by the decomposition of hydrogen peroxide under alkaline conditions, J. Wood Sci. 48 (2002) 191–196, https://doi.org/10.1007/BF00771366.
[58] M. Nielsen, Efficient hydrogen peroxide decomposition to oxygen and water catalysed by a ruthenium pincer complex, Environ. Chem. Lett. 14 (2016) 359–365, https://doi.org/10.1007/s10311-016-0576-0.
[59] E.V. Rokhina, E.A. Golovina, H. van As, J. Virkutyte, ESR ST study of hydroxyl radical generation in wet peroxide system catalyzed by heterogeneous ruthenium, Chemosphere 77 (2009) 148–150, https://doi.org/10.1016/j.chemosphere.2009.05.006.
[60] C.C. Lin, F.R. Smith, N. Ichikawa, T. Baba, M. Itow, Decomposition of hydrogen peroxide in aqueous solutions at elevated temperatures, Int. J. Chem. Kinet. 23 (1991) 971–987, https://doi.org/10.1002/kin.550231103.
[61] M. Thommes, K. Kaneko, A.V. Neimark, J.P. Olivier, F. Rodriguez-Reinoso, J. Rouquerol, et al., Physisorption of gases, with special reference to the evaluation of surface area and pore size distribution (IUPAC Technical Report), Pure Appl. Chem. 87 (2015) 1051–1069, https://doi.org/10.1515/pac-2014-1117.
[62] Schroeder S.L.M., Gottfried M. Temperature-Programmed Desorption (TPD) Thermal Desorption Spectroscopy (TDS). 2002.
[63] M.J. Lashaki, M. Fayaz, H. Wang, Z. Hashisho, J.H. Philips, J.E. Anderson, et al., Effect of adsorption and regeneration temperature on irreversible adsorption of organic vapors on beaded activated carbon, Environ. Sci. Technol. 46 (2012) 4083–4090, https://doi.org/10.1021/es3000195.
[64] A.N. Buckley, R. Woods, X-ray photoelectron spectroscopy of oxidized pyrrhotite surfaces, Appl. Surf. Sci. 22–23 (1985) 280–287, https://doi.org/10.1016/0378-5963(85)90061-3.
[65] Smart R.S.C., Amarantidis J., Skinner W.M., Prestidge C.A., Vanier L.La, Grano S.R. Surface Analytical Studies of Oxidation and Collector Adsorption in Sulfide Mineral Flotation. n.d.
[66] S.S. Kim, L. Britcher, S. Kumar, H.J. Griesser, XPS Study of Sulfur and Phosphorus Compounds with Different Oxidation States, Sains Malays. 47 (2018) 1913–1922, https://doi.org/10.17576/jsm-2018-4708-33.
[67] Castner D.G., Hinds K., Grainger D.W. X-ray Photoelectron Spectroscopy Sulfur 2p Study of Organic Thiol and Disulfide Binding Interactions with Gold Surfaces. 1996.